Journal of Rock Mechanics and Geotechnical Engineering 14 (2022) 82–92

Contents lists available at ScienceDirect

Journal of Rock Mechanics and Geotechnical Engineering

journal homepage: www.jrmge.cn

Full Length Article

Physical model simulation of rock-support interaction for the tunnel in squeezing ground

Ketan Arora*, Marte Gutierrez, Ahmadreza Hedayat

Civil and Environmental Engineering, Colorado School of Mines, Golden, CO, 80401, USA

ARTICLE INFO

Article history:
Received 9 November 2020
Received in revised form
5 July 2021
Accepted 19 August 2021
Available online 1 December 2021

Keywords:
Squeezing ground
Tunnel support system
Longitudinal displacement profile
Rock-support interaction

ABSTRACT

The existence of squeezing ground conditions can lead to significant challenges in designing an adequate support system for tunnels. Numerous empirical, observational and analytical methods have been suggested over the years to design support systems in squeezing ground conditions, but all of them have some limitations. In this study, a novel experimental setup having physical model for simulating the tunnel boring machine (TBM) excavation and support installation process in squeezing clay-rich rocks is developed. The observations are made to understand better the interaction between the support and the squeezing ground. The physical model included a large true-triaxial cell, a miniature TBM, laboratory-prepared synthetic test specimen with properties similar to natural mudstone, and an instrumented cylindrical aluminum support system. Experiments were conducted at realistic in situ stress levels to study the time-dependent three-dimensional tunnel support convergence. The tunnel was excavated using the miniature TBM in the cubical rock specimen loaded in the true-triaxial cell, after which the support was installed. The confining stress was then increased in stages to values greater than the rock's unconfined compressive strength. A model for the time-dependent longitudinal displacement profile (LDP) for the supported tunnel was proposed using the tunnel convergence measurements at different times and stress levels. The LDP formulation was then compared with the unsupported model to calculate the squeezing amount carried by the support. The increase in thrust in the support was back-calculated from an analytical solution with the assumption of linear elastic support. Based on the test results and case studies, a recommendation to optimize the support requirement for tunnels in squeezing ground is proposed.

1. Introduction

After excavation, tunnel wall convergence is a function of the in situ stresses and the behavior of the rock mass at the tunnel location. In squeezing ground conditions, the tunnel converges significantly and continuously with time during or even after the tunnel excavation. As the tunnel converges with time, the loads applied to the tunnel support system increase, resulting in severe stability issues in some cases. Therefore, estimation of the interactions between the rock mass and the tunnel support system (or rock-support interaction) with time is essential to counter the squeezing.

In tunneling, rock-support interaction is used as a preliminary tool for assessing the tunnel support system's behavior during both the design and construction process (Panet, 1995; Carranza-Torres and Fairhurst, 2000; Gschwandtner and Galler, 2012). Several practices were reported in the literature to carry out rock-support interaction (Fenner, 1938; Pacher, 1964; Lombardi, 1975; Brown et al., 1983; Corbetta et al., 1991; Duncan-Fama, 1993; Panet, 1993, 1995; Peila and Oreste, 1995; Carranza-Torres and Fairhurst, 2000; Alejano et al., 2009; Vrakas and Anagnostou, 2014; Cai et al., 2015; Cui et al., 2015; Lü et al., 2017; Pandit and Babu, 2021; Zhang and Nordlund, 2021). Most of the proposed solutions are based on simplifying the three-dimensional (3D) into a two-dimensional (2D) plane-strain problem. A typical example of this approach is the convergence-confinement method (CCM), which has three basic components: (i) the ground reaction curve (GRC), (ii) the longitudinal displacement profile (LDP) of the tunnel, and (iii) the support characteristic curve (SCC). The GRC defines the relationship between the decreasing internal pressure in the tunnel

* Corresponding author.
E-mail address: karora@aldeaservices.com (K. Arora).
Peer review under responsibility of Institute of Rock and Soil Mechanics, Chinese Academy of Sciences.

https://doi.org/10.1016/j.jrmge.2021.08.016

and the increase in tunnel convergence. The LDP is the plot of the tunnel convergence that occurs along the tunnel axis as a function of the distance from the tunnel face. The SCC expresses the relationship between the increasing stresses on the tunnel support and the increasing support displacement.

Conventional CCM considers the tunnel deformation only based on the tunnel's advancement and the change in the internal pressure. However, the tunnel also converges with time and even after the excavation is complete in squeezing ground conditions. This time-dependent convergence can generate additional stresses in the tunnel support system and can ultimately cause unpredictable support failures, construction hazards, cost overruns, and project delays (Paraskevopoulou and Benardos, 2013).

The only approach reported in the literature that developed CCM for squeezing ground conditions incorporates a time-dependent rock mass model for a tunnel (Paraskevopoulou and Diederichs, 2018). The time-dependent behavior was explicitly studied for the rock mass (Paraskevopoulou and Diederichs, 2018) or indirectly by monitoring the change in stresses on the tunnel support (Gschwandtner and Galler, 2012). The former approach modifies the LDP with time using a time-dependent constitutive model while assuming the rock mass's visco-elastic behavior. On the other hand, the latter approach predicts the increase in stresses applied to the support system in the excavated tunnel based on the field monitoring data. Given that the change in stresses applied to the tunnel support system is monitored for a real project, this latter approach can be more accurate than the first approach. However, due to high levels of applied loads and deformations, the field sensors (just like the tunnel support system themselves) experience extreme environments and often fail before meaningful data can be measured once the squeezing has started. Without reliable field data, it is challenging to develop a CCM to calculate the tunnel support stresses. This is the primary reason why tunnel designers mostly rely on empirical equations derived from limited field observations for tunnels in squeezing ground conditions, as discussed in Arora et al. (2021c). Since in situ monitoring is often limited in squeezing environments, realistic physical model tests can provide valuable information to evaluate better the interaction between the support and the squeezing ground (Lin et al., 2015).

This paper aims to provide a comparison between the LDPs of supported and unsupported tunnels using carefully conducted laboratory-scale physical model tests in squeezing ground. The experiment involved tunnel boring machine (TBM) excavation and support installation in a synthetic mudstone specimen, with squeezing and time-dependent behavior, under increasing in situ stresses. The physical model test explored the critical aspects of tunnel excavation, such as the tunnel advancement, the 3D effects, the support installation, and the highly plastic and ductile time-dependent behavior of the ground. The experimental observations and results are synthesized in terms of convergence and support stresses at different times and loading levels. Case studies of the tunnels' support systems in squeezing ground conditions are also presented as well as a proposed methodology for the selection of the tunnel support system.

2. Experimental setup

The setup used in this study physically simulated the TBM excavation and tunnel support installation procedure in a cubical rock specimen at field stress levels (up to 550 m overburden due to weight of mudstone) in a true-triaxial cell. More features of the experimental setup are available in Arora et al. (2019, 2020a, b, 2021a). The temporal changes in the liner deformation were monitored and analyzed throughout the experiment.

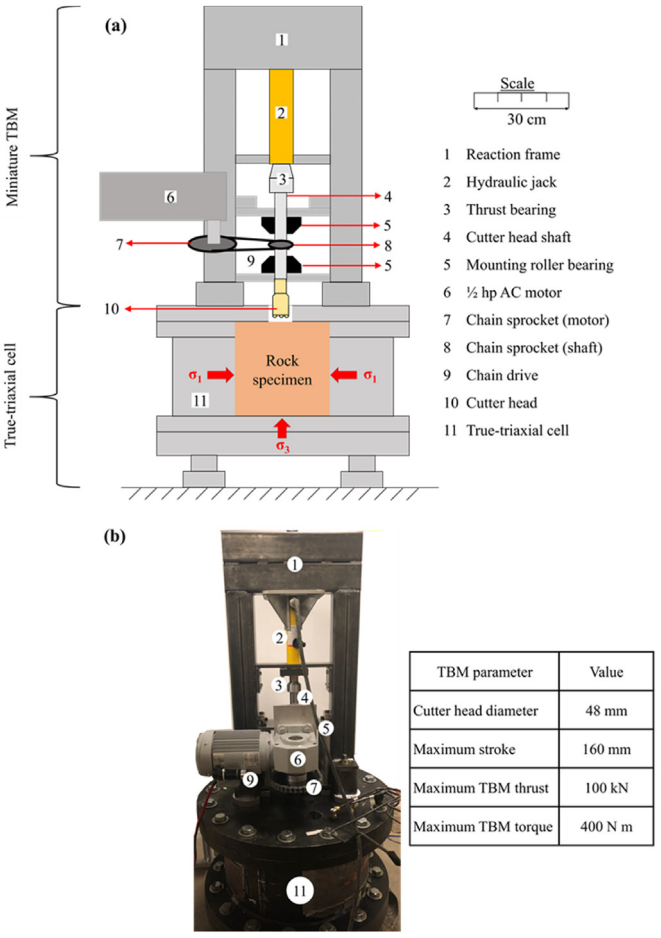

Fig. 1. Experimental arrangement to study tunnels in squeezing ground conditions: (a) Schematic diagram, and (b) Actual setup at Colorado School of Mines.

The experimental setup is illustrated in Fig. 1a, using a schematic diagram. A photograph of the experimental setup at the Colorado School of Mines, where this research was conducted, is provided in Fig. 1b. The experimental setup consists of a true-triaxial cell, a miniature TBM, a cubical synthetic mudstone specimen as the mudstone-like material, the tunnel support system, and the monitoring unit. The important aspects of the test setup and the loading, excavation and support installation details are discussed in the following sections.

2.1. Cubical rock specimen

It is challenging to obtain natural, homogenous and undisturbed specimens of mudstone from the field. Therefore, this study incorporated a synthetic mudstone prepared in the laboratory by mixing cement, clay and water following Arora et al. (2020c). The test material exhibits the characteristics of squeezing clay-rich rock (i.e. ductility even at low confining stresses, extensive plastic deformation, and pronounced time and loading rate dependency).

Arora et al. (2020c) reported that, based on laboratory tests, the mean unconfined compressive strength (UCS) σ_c was 4.47 MPa with a standard deviation of 0.15 MPa, the mean Young's modulus E was 0.65 GPa with a standard deviation of 0.02 GPa with, and the Poisson's ratio ν was 0.13. For the confining stresses varying from 1 MPa to 4 MPa and using the Mohr-Coulomb linear fit, the effective cohesion c and internal friction angle φ were 2.06 MPa and 10°, respectively. During the creep tests, the synthetic mudstone was observed to develop a considerable amount of creep strain with

time (Arora et al., 2020c). The laboratory tests conducted by Arora et al. (2020c) are discussed in Appendix A.

The laboratory test results showed that both the synthetic mudstone as tested and the naturally occurring and squeezing-mudstone have similar shear strength, elastic modulus, ductility, strain-rate sensitivity and creep behavior.

The 300 mm × 300 mm × 300 mm cubical synthetic mudstone specimen was prepared using the same material, composition and procedure given in Arora et al. (2020c). The test specimen made of the mixture of clay, cement and water was removed from the mold after 24 h and further cured in distilled water for 28 d before the testing commenced.

2.2. The loading unit

The physical model test was carried out using a true-triaxial cell developed by Frash et al. (2014) at the Colorado School of Mines. The unique feature is that the drilling activity is carried out in the rock specimen as it is loaded in a true-triaxial stress state, making it suitable to simulate in situ stress conditions. The true-triaxial cell, originally designed to carry out the thermo-mechanical simulation of enhanced geothermal systems, was modified to study TBM-excavated tunnels in squeezing ground conditions by Arora et al. (2020a). The true-triaxial cell applies the confining pressure in each direction using the combination of flexible membrane flat jack and steel platens.

In each one of the loading directions, one face of the rock specimen (active face) makes direct contact with the flat jack while the other face (defined as the passive face) gives the reaction with a rigid plane. The active face has an active hydraulic jack, 300 mm-diameter circular steel platens on each faces of the flat jack, and a 300 mm × 300 mm rectangular steel platen sandwiched between the specimen and the circular steel platen. The rigid passive platen is stationary and made up of concrete. With this arrangement, the apparatus is efficient of applying three independently regulated principal stresses up to 13 MPa to a 300 mm cubical rock specimen. The top lid of the true-triaxial cell is made of steel and equipped with two circular ports of 63 mm and 75 mm in diameter. The smaller 63 mm-diameter port is a pass-through for the sensor cable and hydraulic lines while the larger 75 mm port at the center of the lid provides entry to the surface of the rock specimen for the tunnel excavation using the miniature TBM. Further details about this true-triaxial apparatus can be found in Frash et al. (2014). The revisions for the tunneling experiment presented in this study are given in Arora et al. (2019, 2020a, 2021a).

2.3. Tunnel excavation unit

Numerous researchers have investigated tunnel excavation process using physical model tests by developing a miniature TBM (Nomoto et al., 1999; Wang et al., 2019; Liu et al., 2020). A miniature soft ground open-face TBM was mounted on the true-triaxial cell to excavate a tunnel. At the same time, the cubical rock specimen was loaded in the true-triaxial cell. As the tunnel excavation needed to occur while the rock was subjected to the in situ stress levels, the miniature TBM was designed to provide a sufficient cutter head thrust and torque. The miniature TBM mounted on the top of the true-triaxial cell is given in the conceptual diagram in Fig. 1.

The four key elements of the miniature TBM are the thrust unit, torque unit, cutting unit and supporting unit. The diameter of the cutter head disc is 48 mm, and the maximum 150 mm long tunnel can be excavated with this miniature TBM. A set of Teledyne ISCO syringe pumps and a hydraulic cylinder fulfilled the required face pressure (thrust) for the excavation to the cutter head. The apparatus can apply a face pressure up to 10 MPa. The torque is supplied by a 0.5 hp, 115 V, single-phase, constant speed, alternating current (AC) motor through a chain drive, as presented in Fig. 1. The motor spins at a continuous speed of seven revolutions per minute and is capable of providing a maximum torque of 400 N m.

As shown in Fig. 1, the cutting unit is comprised of a shaft with a cutter head connected at the end. The other end of the shaft is connected to a hydraulic jack by employing a thrust bearing. The miniature TBM was constructed for the excavation of soft rock (e.g. mudstone) and the drill bit had a cutter head with nine button-type tungsten carbide bits. The complete design and working mechanism of the miniature TBM can be found in Arora et al. (2021a).

2.4. Tunnel support system

A thin cylinder made of 6061 aluminum alloy, with 44.5 mm in outer diameter (OD) and 1.65 mm in thickness t_s, was used as the tunnel support system. The ultimate tensile strength, Young's modulus E_s and Poisson's ratio ν_s of the 6061 aluminum were 276 MPa, 68.9 GPa and 0.35, respectively (Zwilsky and Langer, 2001). The annular gap between the support system and the tunnel boundary measured 1.5 mm and was filled with non-shrinking grout and cured for 3 d. The 3-d compressive strength of this grout was 1.12 MPa, which is the same as σ_c. It is reasonable to assume that the grout, similar to the real backfill grout in tunnels, played its intended role in transferring the ground loads to the support system considering the strength difference between the grout and the aluminum material.

Fig. 2a schematically shows the cubical rock specimen with the tunnel loaded in the true-triaxial cell. Fig. 2b shows the support system with strain gauges in the tangential direction. The strain gauges' position on the tunnel support from the longitudinal view is shown in Fig. 2c, and the cross-sectional view is shown in Fig. 2d.

3. Test procedures

After 28 d of curing in water, the cubical synthetic mudstone specimen was loaded in the true-triaxial cell. The rock specimen was first subjected to a low isotropic compressive stress $p_o = 0.5\sigma_c$. Then, a tunnel of 48 mm in diameter and 140 mm in length was excavated in the rock specimen using the miniature TBM with longitudinal axis along the x-axis of the coordinate system, as shown in Fig. 2a.

After the grout cured for 3 d, the isotropic stress p_o was applied in five stages over 605 h, as shown in Fig. 3. The complete time of loading and monitoring was decided based on the beginning of the steady-state (i.e. the rock specimen was loaded until the strain in the tunnel support hit the steady-state). The five loading stages of this test are defined as follows:

(1) Loading stage I: After excavating the tunnel and installing the tunnel support, p_o was increased from $0.5\sigma_c$ to σ_c. As shown in Fig. 3, points A and B are the beginning and end of the loading stage I, respectively. The total loading stage time was 125 h and p_o was equal to σ_c.
(2) Loading stage II: At the end of the loading stage I, p_o was increased rapidly from σ_c (point B) to $1.5\sigma_c$ (point C), as shown in Fig. 3. Point C indicates the beginning of loading stage II, and after 120 h, point D marks the end, as shown in Fig. 3.
(3) Loading stage III: The isotropic stress on the cubical rock specimen was further increased by $0.5\sigma_c$, making $p_o = 2\sigma_c$. The total time of loading for this stage was 120 h. The beginning and the endpoint of this loading stage are points E and F in Fig. 3.

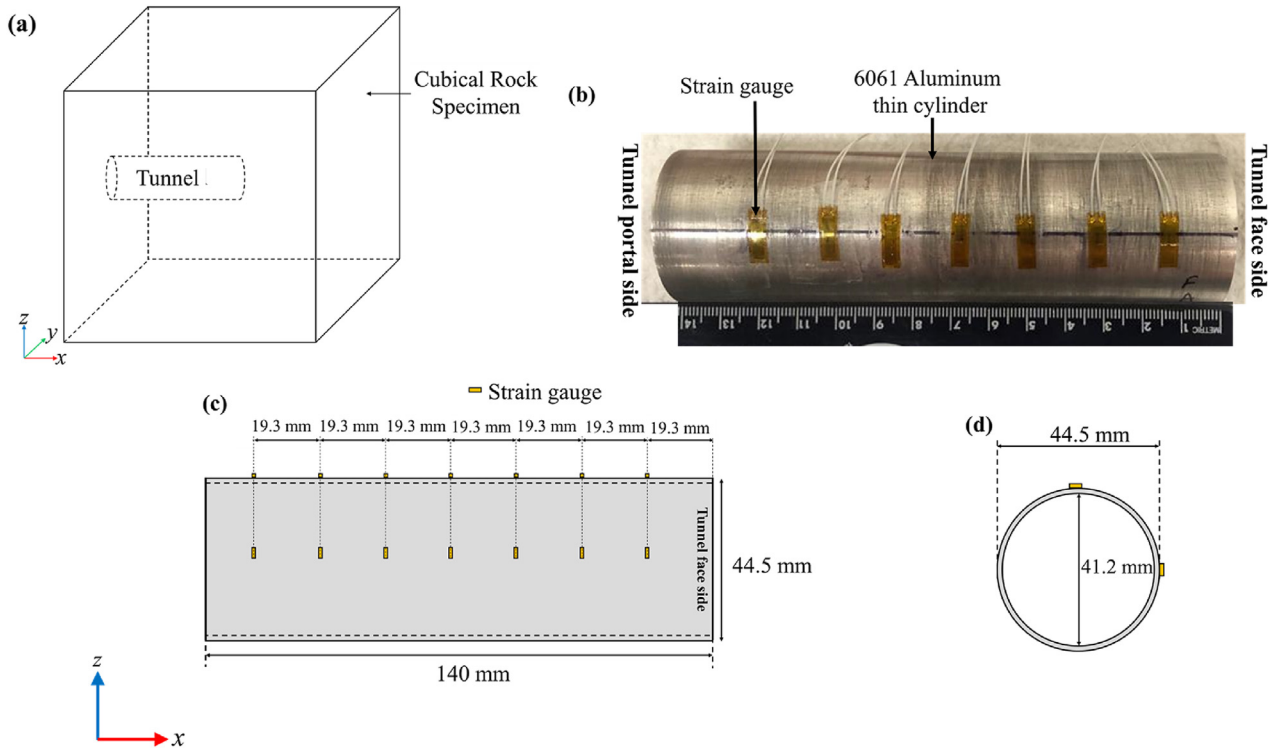

Fig. 2. (a) Schematic diagram of cubical rock specimen in true-triaxial stress state with tunnel, (b) Aluminum tunnel support with strain gauges in tangential direction, (c) Longitudinal view of the tunnel support system along with position of strain gauges, and (d) Cross-section of the tunnel support system.

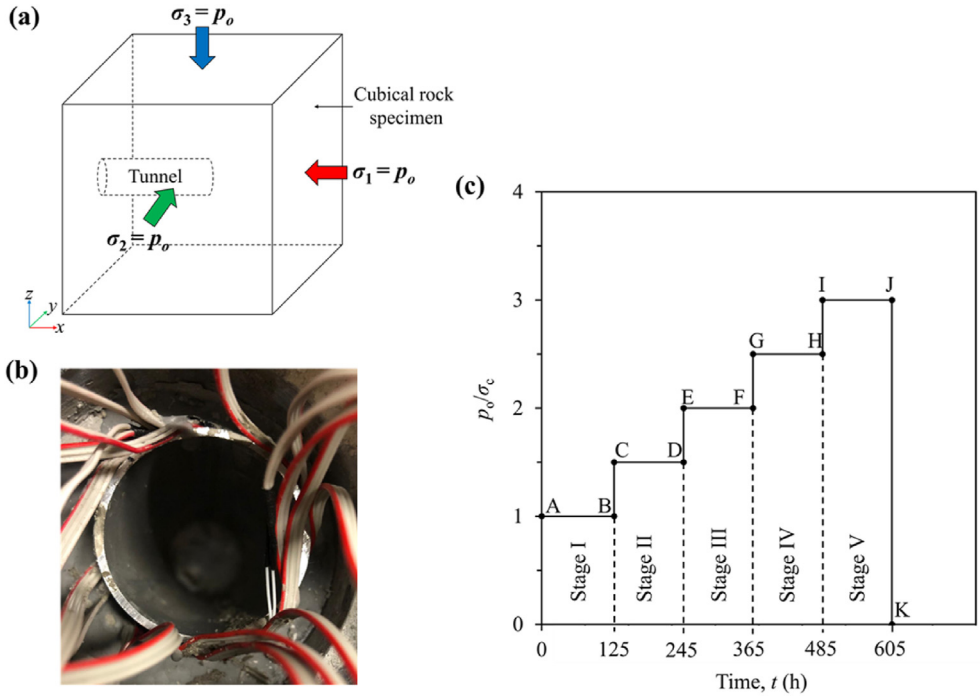

Fig. 3. (a) Conceptual diagram of the cubical rock specimen with tunnel loaded in true-triaxial stress, (b) Support placed inside the tunnel, and (c) Isotropic stress ratio applied on a cubical rock specimen during the five loading stages.

(4) Loading stage IV: In this loading stage, p_o was increased by $0.5\sigma_c$ and kept constant for another 120 h while monitoring tunnel support behavior.
(5) Loading stage V: In this final loading stage, p_o was further increased from $2.5\sigma_c$ to $3\sigma_c$. The rock specimen was loaded for 120 h and finally unloaded to reach $p_o = 0$ MPa.

4. Experimental observations and results

4.1. Tunnel excavations in three phases

Fig. 4 shows the 48-mm diameter tunnel response after it was excavated in three phases, lasting 19.5 h. As shown in Fig. 4a, the

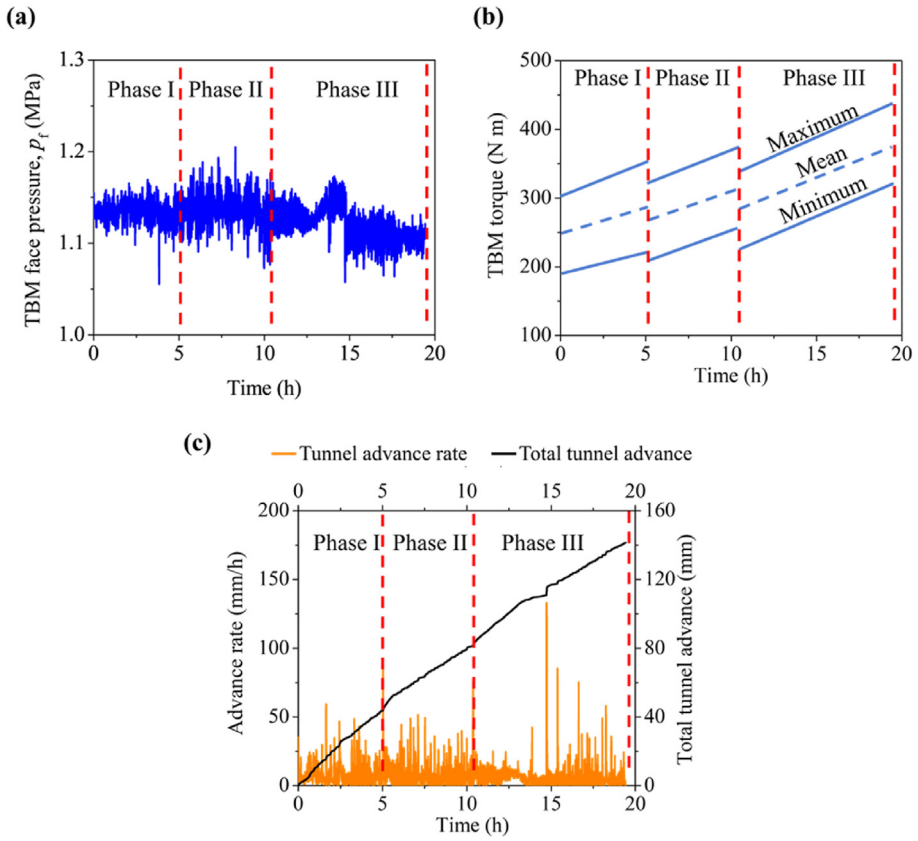

Fig. 4. Monitoring of miniature TBM parameters during the excavation stage: (a) Face pressure (thrust), (b) TBM torque, and (c) TBM advancement and the advance rate.

mean TBM face pressure p_f applied to the tunnel face via the cutter head throughout the excavation stage was about 1.12 MPa with a standard deviation of 0.05 MPa. The isotropic stress p_o applied on the cubical rock specimen was $0.5\sigma_c$, roughly two times that of p_f. The miniature TBM shaft rotated at a constant speed of 13 revolutions per minute, and the torque output was continuously monitored, as shown in Fig. 4b.

During Phase I of the excavation, a 42-mm long tunnel was excavated in 5 h, followed by removing the cut material. It was observed that when the cut material was not removed efficiently, the tunnel became clogged, and the advance rate significantly slowed down, as shown in Fig. 4c. Phase II of the tunnel excavation began after the cut material of Phase I was removed. In this stage, a 38-mm long tunnel was excavated in 5.3 h, making the total length of the tunnel 80 mm. In the last stage of the excavation, the tunnel further advanced by 60 mm in 9.2 h, making the full length of the tunnel 140 mm.

4.2. Support deformations

Throughout the experiment, the tunnel support behavior was monitored by the tangential strain gauges on the support system, as shown in Fig. 2c. The strain gauges were installed on the outer surface of the cylinder in contact with the grout. It was assumed that at the point of contact, the strains in the rock and support were the same, considering the continuity of the tangential strain at this interface. The tangential strain at the tunnel boundary is the ratio of tunnel convergence u to its radius R. Hence, the strain gauges on the support provide the LDP of the supported tunnel at any given p_o and time.

This section discusses the change in the LDP of the supported tunnel with time during the five loading stages shown in Fig. 3. Displacement u and the longitudinal distance from the tunnel face x_f were normalized with tunnel radius R to present the most common form results. Ratio u/R (in %) is effectively the tunnel wall radial strain, and parameter $X = x_f/R$ is the normalized longitudinal distance from the tunnel face.

Fig. 5 shows the selected but representative LDP readings (u/R versus X plot) of the tunnel over the time for all five loading stages. Due to squeezing, the LDP of the tunnel was observed to shift upwards with time. Of the five tunnel sections studied, the LDP's maximum and minimum upward shifts with time were recorded at $X = 4.5$ and 0.9, respectively, throughout the test. The corresponding increases in u/R at $X = 4.5$ for loading stages I to V due to squeezing were 0.005%, 0.125%, 0.13%, 0.166% and 0.452%, respectively. However, the increases in u/R at $X = 0.9$ were relatively low and were recorded as 0.001%, 0.038%, 0.055%, 0.074% and 0.091% during loading stages I to V, respectively.

5. A time-dependent LDP

The most widely used LDPs for unsupported tunnels were proposed by Panet (1995) and Vrakas and Anagnostou, 2014. Due to the rock's time-dependent behavior, the stresses on the tunnel support increase with time in squeezing ground conditions. The complications reported in the literature regarding the application of CCM in squeezing ground were discussed in this paper. However, the study presented here deals with the direct monitoring of the tunnel support response in squeezing ground conditions subjected to different in situ stress levels. Hence, a time-dependent LDP of the

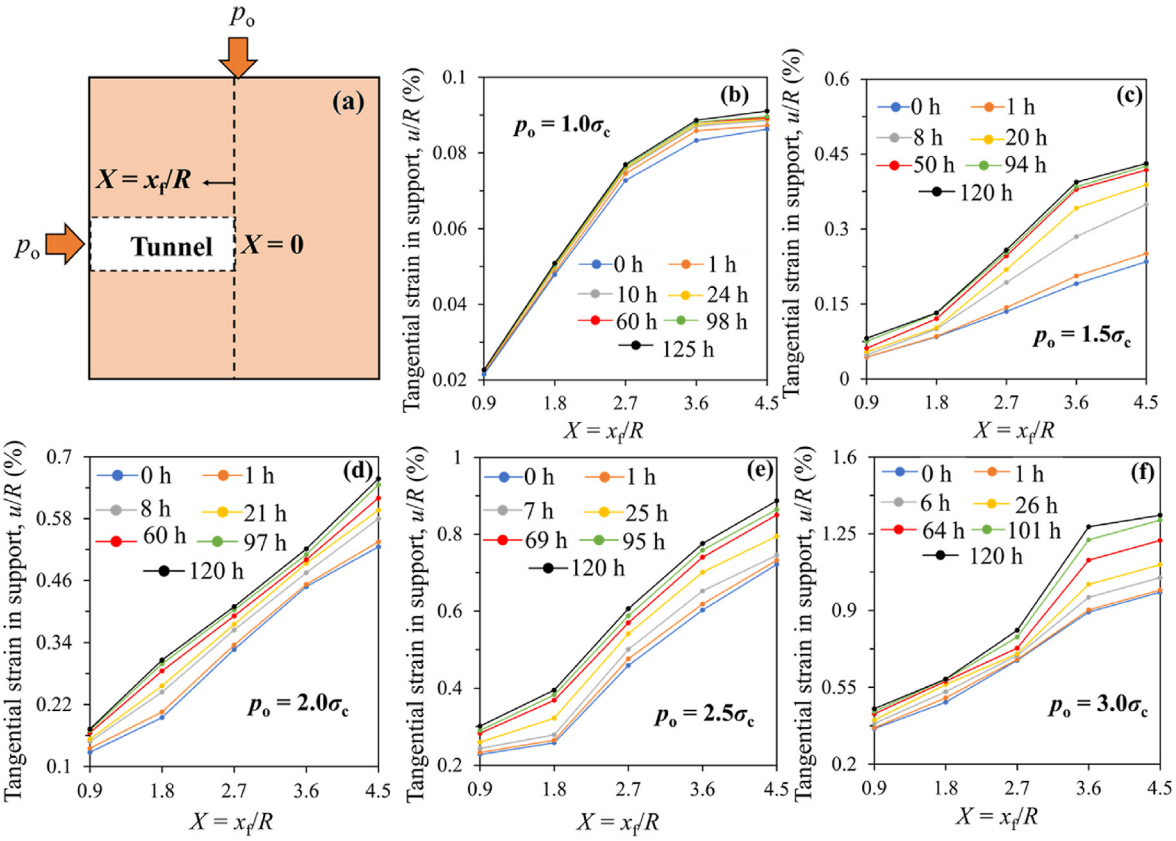

Fig. 5. (a) Longitudinal tunnel excavated in isotropic stress state, and LDP of the tunnel at the different times for the loading stages (b) I, (c) II, (d) III, (e) IV and (f) V.

supported tunnel was chosen to simplify the study of tunnel support behavior in squeezing ground conditions.

Fig. 6 depict the tangential strain changes as a function of the loading stage time t for the five loading stages for five equally spaced longitudinal tunnel sections ranging from $X = 0.9$ to 4.5. It also can be seen that for any tunnel section and during any loading stage, the correlation between tunnel strain u/R in % and time t in h could be expressed as an asymptotic model and given by the following equation:

$$\frac{u}{R}(t) = a_s - b_s(d_s)^t \tag{1}$$

where a_s, b_s and d_s are the model parameters determined from the best fitting curve having the maximum coefficient of determination with the experimental data. The best fit values of the model parameters a_s, b_s and d_s for all the plots and the coefficient of determination are shown in Table 1.

Parameter d_s governs the supported tunnel's time-dependent response, and from the test observations, it can be considered constant as $d_s = 0.98$. As shown in Table 1, the parameter a_s increases with increases in X and p_o/σ_c. Table 1 also indicates that parameter b_s increases with an increase in p_o/σ_c but shows a weak correlation with X. Hence, the a_s can be expressed as the function of p_o/σ_c and X as follows:

$$a_s = f\left(\frac{p_o}{\sigma_c}, X\right) \tag{2}$$

where f is the function of p_o/σ_c and X. Fig. 7 shows the dependency of parameter a_s on p_o/σ_c and X. It can be observed in Fig. 7 that for a given p_o/σ_c, a_s increases almost linearly with increase in X. The parameter b_s was found increase with increase in p_o/σ_c and can be expressed as

$$b_s = g\left(\frac{p_o}{\sigma_c}\right) \tag{3}$$

where g is the function of p_o/σ_c. Eq. (1) can be rewritten as

$$\frac{u}{R}(t) = f\left(\frac{p_o}{\sigma_c}, X\right) - g\left(\frac{p_o}{\sigma_c}\right)(d_s)^t \tag{4}$$

According to Eq. (1), parameter a (for $d_s < 1$) can be defined for any tunnel section as the tunnel strain at an infinite time as follows:

$$\frac{u}{R}(t \to +\infty) = a_s \tag{5}$$

Also, according to Eq. (1), the difference between parameters a_s and b_s is the tunnel strain at the beginning of any loading stage ($t = 0$):

$$\frac{u}{R}(t = 0) = a_s - b_s \tag{6}$$

5.1. Effect of support system on the LDP

In addition to the influences of p_o/σ_c and X, the LDP was also influenced by the support systems by comparing the LDP of the supported and unsupported tunnels, as discussed in Arora (2020) and Arora et al. (2021b). It was determined that the support system influences the instantaneous and long-term convergences of the tunnel.

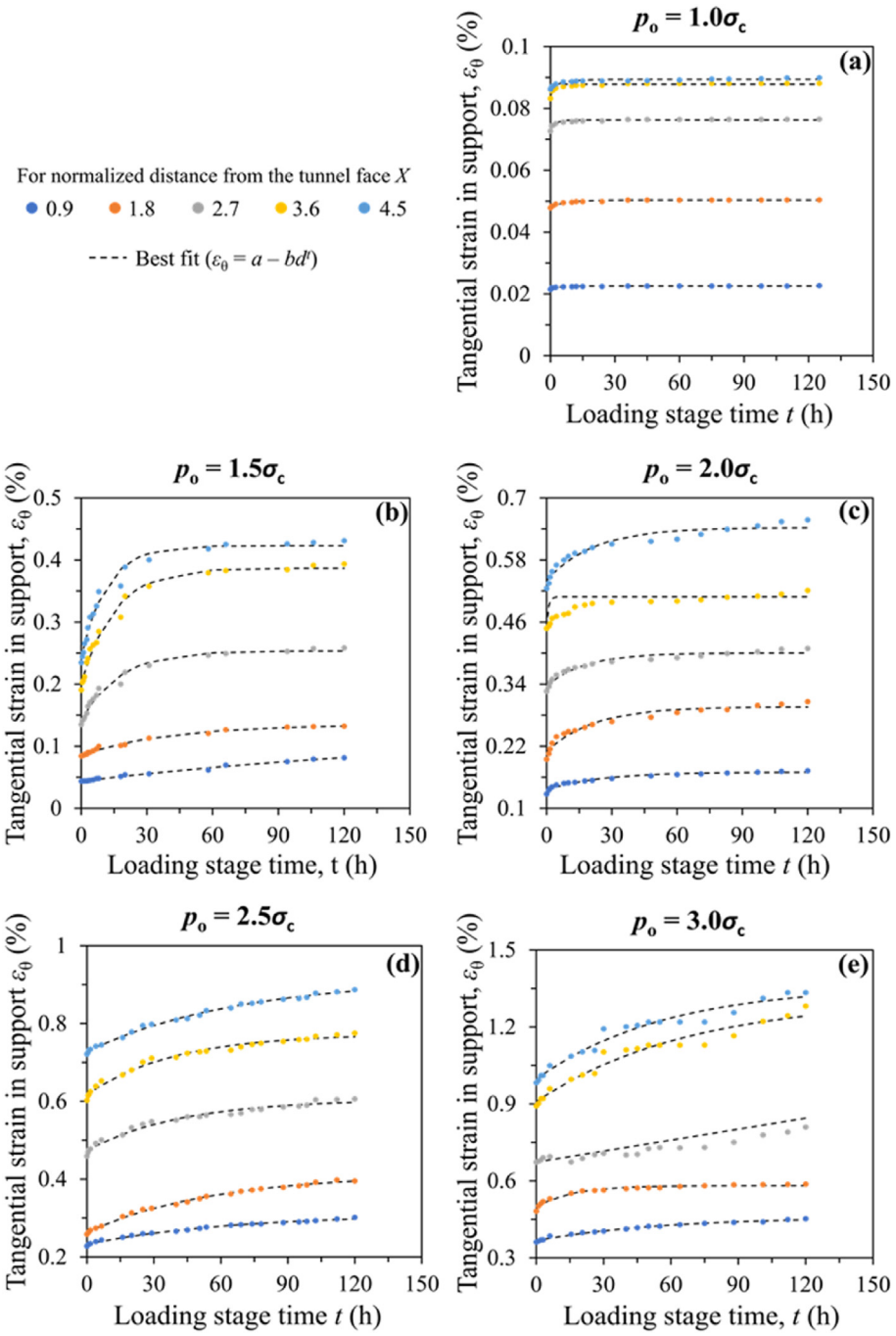

Fig. 6. Tunnel strain u/R (in %) with loading stage time t for X varying from 0.9 to 4.5 for loading stages (a) I, (b) II, (c) III, (d) IV and (e) V.

The change in u/R in percentage at $t = 0$ due to support installation, calculated using Eq. (6), is given by

$$\Delta\left(\frac{u}{R}\right)_{\text{instant}} = \frac{(a-b)-(a_s-b_s)}{a-b} \times 100\% \tag{7}$$

Similarly, the percentage change in u/R at an infinite time due to support installation, calculated using Eq. (5), is given by

$$\Delta\left(\frac{u}{R}\right)_{\text{ultimate}} = \left(\frac{a-a_s}{a}\right) \times 100\% \tag{8}$$

Parameters a, b and d for an unsupported tunnel for different loading stages are provided in Table 1, as discussed in Arora (2020). The parameters in Table 1 were used to calculate $\Delta(u/R)_{\text{instant}}$ and $\Delta(u/R)_{\text{ultimate}}$. The installed tunnel support reduced the instantaneous and ultimate tunnel convergences by 96%–98% for all cross-sections and loading conditions.

5.2. Load applied to the support system

Throughout the experiment, the tunnel support strains increased with time due to squeezing ground. Given its modulus and dimensions, the support system did not reach the yielding stage and remained linear elastic throughout the test. Hence, it can be stated that the stresses on the tunnel support also increased

Table 1
LDP model parameters for supported and unsupported tunnels.

p_o/σ_c	$X = x_f/R$	Supported tunnel				Unsupported tunnel*		
		a_s	b_s (10^{-3})	d_s	Coefficient of determination	a	b	d
1	0.9	0.02	0.85	0.76	0.87	2.43	1.22	0.98
	1.8	0.05	2.21	0.87	0.96	2.92		
	2.7	0.08	3.02	0.66	0.89	3.41		
	3.6	0.09	4.1	0.5	0.88	3.90		
	4.5	0.09	2.68	0.85	0.88	4.39		
1.5	0.9	0.13	82.96	0.99	0.99	5.45	2.65	
	1.8	0.13	49.49	0.98	0.99	5.95		
	2.7	0.25	112.78	0.94	0.98	6.46		
	3.6	0.39	86.37	0.94	0.99	6.97		
	4.5	0.42	180.89	0.92	0.98	7.48		
2	0.9	0.17	34.51	0.96	0.95	11.65	4.59	
	1.8	0.3	86.7	0.95	0.94	12.22		
	2.7	0.4	64.07	0.95	0.94	12.8		
	3.6	0.51	56.85	0.93	0.94	13.37		
	4.5	0.64	102.31	0.95	0.93	13.94		
2.5	0.9	0.31	76.97	0.98	0.99	20.65	7.04	
	1.8	0.41	149.99	0.98	0.99	21.3		
	2.7	0.61	131.83	0.98	0.97	21.94		
	3.6	0.77	156.29	0.97	0.98	22.59		
	4.5	0.92	187.74	0.99	0.99	23.24		
3	0.9	0.46	92.09	0.98	0.99	32.76	9.98	
	1.8	0.58	84.65	0.94	0.96	33.51		
	2.7	0.93	251.48	0.98	0.92	34.27		
	3.6	1.31	401.45	0.99	0.95	35.02		
	4.5	1.36	366.36	0.98	0.96	35.78		

Note: * The values presented in the table are extracted from the LDP model for the unsupported tunnel proposed by Arora (2020).

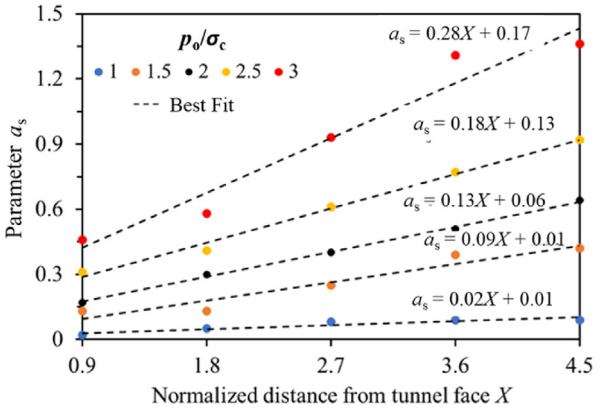

Fig. 7. Change in the model parameter a_s with change in p_o/σ_c and normalized distance from the tunnel face.

linearly with the increase in measured strains. These stresses can be calculated from the analytical solution of the tunnel support system given by Schwartz and Einstein (1980), which considers that the tunnel boundary transfers bending and thrust forces to the tunnel support. The convergence of the tunnel support is a combined effect of the bending and thrust given by the following equations for the full slip condition (no shear stress) between the rock and the support, and the tunnel excavated in an isotropic stress state:

$$\frac{T}{PR} = (1 - a_o^*) \tag{9}$$

$$\frac{M}{PR^2} = 0 \tag{10}$$

$$\frac{u}{R} = P\left(\frac{1+\nu_g}{E_g}\right)a_o^* \tag{11}$$

where P is the ground stress acting on the support, T is the thrust force on the support, and M is the bending moment on the support and is zero in isotropic stress conditions (Schwartz and Einstein, 1980). The parameters E_g and ν_g are the Young's modulus and Poisson's ratio of the rock, respectively. Parameter a_o^* is the function of compressibility ratio C^* and flexibility ratio F^* of the rock and support given by the following equations:

$$a_o^* = \frac{C^*F^*(1-\nu_g)}{C^* + F^* + C^*F^*(1-\nu_g)} \tag{12}$$

$$C^* = \frac{E_g R(1-\nu_s^2)}{E_s A_s\left(1-\nu_g^2\right)} \tag{13}$$

$$F^* = \frac{E_g R^2(1-\nu_s^2)}{E_s I_s\left(1-\nu_g^2\right)} \tag{14}$$

$$I_s = \frac{t_s^3}{12} \tag{15}$$

$$A_s = t_s \tag{16}$$

where E_s and ν_s are the Young's modulus and Poisson's ratio of the support, respectively; and I_s and A_s are the moment of inertia per unit length of the support cross-section about its centerline and the area of the support per unit length experiencing the thrust and moment, respectively.

Combining Eqs. (9) and (11) to calculate T for a given u in the following equation is

$$T = \frac{uE_g}{(1+\nu_g)a_o^*}(1 - a_o^*) \tag{17}$$

Using Eq. (17), thrust forces T at the start and end of each loading cycle are presented in Table 2. As can be seen, except during loading stage I, the thrust on the support increased significantly during loading stages II through V. This additional increase in T with time was the result of the added squeezing of the rock.

6. Case studies

Parameters a_s, b_s and d_s of the LDP determined from this model study depend on the rock elastic properties, the support elastic properties and its geometry. However, exploring the individual effects of the involved parameters requires numerous tests, which may not always be feasible. One feasible approach to account for the rock and support system variations is to utilize the compressibility ratio C^* and flexibility ratio F^* concept, given in Eqs. (13) and (14), respectively.

The support system used in this study reduced the time-dependent convergence of the tunnel by 96% compared to the unsupported tunnel. The C^* and F^* for the conducted test determined from Eqs. (13) and (14) are 0.11 and 0.24, respectively. For the unsupported tunnels, C^* and F^* both approached infinity. Additional information on the convergence of the supported tunnels with different C^* and F^* values would be required to optimize the support requirements. In this paper, the knowledge is expanded by carrying out the case studies of the tunnel support response

Table 2
Thrust in the tunnel support at the beginning and end of different loading stages.

$X = x_f/R$	Thrust on support, T (kN/m)									
	Stage I ($p_o = \sigma_c$)		Stage II ($p_o = 1.5\sigma_c$)		Stage III ($p_o = 2\sigma_c$)		Stage IV ($p_o = 2.5\sigma_c$)		Stage V ($p_o = 3\sigma_c$)	
	Beginning	End	Beginning	End	Beginning	End	Beginning	End	Beginning	End
0.9	28	29	57	106	166	224	296	391	469	587
1.8	62	66	109	172	253	397	335	513	626	762
2.7	94	100	175	335	424	531	596	787	874	1051
3.6	108	115	247	511	581	676	782	1006	1158	1663
4.5	112	118	305	559	682	853	936	1151	1275	1732

under squeezing conditions. The case studies are summarized in Table 3 and presented as follows.

6.1. Laodongshan railway tunnel in China

This tunnel, a part of the Guangzhou-Kunming railway in China, experienced squeezing failure in its early construction stage due to excavation in weak mudstone at high in situ stresses (Cao et al., 2018). Four primary tunnel support systems were tested at a critical cross-section. The influence of the long-term convergence at the crown was studied to optimize the support requirements. The four support systems in the order of decreasing C^* (see Table 3) were I20a steel at 0.8-m spacing, I22b steel at 0.6-m spacing, H175 steel at 0.6-m spacing and H200 steel at 0.6-m spacing. It was concluded from the field monitoring of Cao et al. (2018) that the tunnel cross-section with a support system having higher C^* experienced less convergence due to squeezing. Table 3 presents the percent change in tunnel convergence $\Delta(u/R)_{ultimate}$ for the four tested tunnel support systems calculated from the observations of Cao et al. (2018).

6.2. John street pumping station tunnel

The John street pumping station tunnel, built in 1925, supplies the water to downtown Toronto, Canada. A new tunnel was constructed to help with a water supply and the existing tunnels (Czurda et al., 1973). It was constructed in weak squeezing mudstone with the horizontal stresses between 13 and 30 times the vertical stresses (Lo et al., 1987). A 39.5-cm thick steel tube and the concrete composite liner was installed to prevent the considerable convergence due to squeezing. Table 3 presents the C^* and $\Delta(u/R)_{ultimate}$ calculated for the John street pumping station tunnel from Lo et al. (1987).

6.3. 'Wished-in-place' tunnel with polyvinyl chloride (PVC) liner

Arora et al. (2020b) carried out a physical model test on a synthetic mudstone specimen using the true-triaxial setup discussed earlier in this paper. However, unlike the present study, the cubical sample of the synthetic mudstone had a 'wished-in-place' tunnel with PVC liner as a support system. Based on the experimental observations in Arora et al. (2020b), it was observed that the PVC liner reduced the convergence of the tunnel by 87%. The PVC liner properties, C^* and $\Delta(u/R)_{ultimate}$ are shown in Table 3.

7. Support selection criterion

Fig. 8 shows the plot of $\Delta(u/R)_{ultimate}$ versus C^* for the discussed case studies and the experimental observations in this paper. Based on the observations, the relationship between $\Delta(u/R)_{ultimate}$ versus C^* can be expressed by

$$\Delta\left(\frac{u}{R}\right)_{ultimate} = 100\exp(-0.033C^*) \tag{18}$$

For a very stiff support ($C^* = 0$), from Eq. (18), $\Delta(u/R)_{ultimate}$ is 100. Also, for unsupported tunnels, C^* is infinity and the corresponding $\Delta(u/R)_{ultimate}$ is 0.

The methodology for the selection of the efficient and economic tunnel support system in squeezing ground conditions using Eq. (18) is as follows:

(1) Step 1: Determine the ultimate convergence of the unsupported tunnel $(u/R)_{unsupported}$ from the field monitoring. However, in most of the squeezing tunnels, it is almost impossible to obtain reliable data from the field monitoring. Therefore, in such cases, $(u/R)_{unsupported}$ can be obtained from the in situ stress p_o and compressive strength of the rock mass at the tunnel location using the equation proposed by Hoek and Marinos (2000) as

$$\left(\frac{u}{R}\right)_{unsupported} = 0.2\left(\frac{\sigma_{cm}}{p_o}\right)^{-2} \tag{19}$$

(2) Step 2: Determine $\Delta(u/R)_{ultimate}$ using the following equation:

$$\Delta\left(\frac{u}{R}\right)_{ultimate} = \left(\frac{u}{R}\right)_{unsupported} - \left(\frac{u}{R}\right)_{desired} \tag{20}$$

where $(u/R)_{desired}$ is the maximum allowable convergence selected by the tunnel designer.

(3) Step 3: From Eq. (18), determine C^* for the $\Delta(u/R)_{ultimate}$ obtained in Step 2.

Table 3
Case studies of the tunnel support in squeezing ground conditions.

Project	Support type	E_s (GPa)	ν_s	A_s (cm^2/cm)	E_g (GPa)	ν_g	R (cm)	C^*	$\Delta(u/R)_{ultimate}$ (%)
Laodongshan railway tunnel in China (Cao et al., 2018)	Support #1: I20a steel at 0.8-m spacing	200	0.3	0.445	3.18	0.35	600	22.24	45
	Support #2: I22b steel at 0.6-m spacing			0.775				12.77	59
	Support #3: H175 steel at 0.6-m spacing			0.857				11.55	79.6
	Support #4: H200 steel at 0.6-m spacing			1.059				9.35	82.2
Experiment (Arora et al., 2020b)	'Wished-in-place' tunnel with PVC liner	2.89	0.32	0.395	0.69	0.13	2.21	1.22	87.23
John street pumping stating tunnel, Canada (Czurda et al., 1973; Lo et al., 1987)	Composite steel tube and concrete	20	0.2	39.5	3	0.15	112.5	0.42	94
Present study	Aluminum	69.9	0.35	0.165	0.69	0.13	2.06	0.11	96

(4) Step 4: Using Eq. (13), select the most suitable combination of Young's modulus of support E_s and cross-sectional area A_s that will not give C^* more than obtained in Step 3.

8. Discussions

8.1. Observation time for squeezing

The observation time in each loading stage presented in this paper was 7 d while squeezing may continue for weeks or even months after the excavation. The criterion proposed is based on 7 d of monitoring and the observations are extrapolated to infinite time. However, in future, the developed technique will need to be calibrated with the long-term field observations of the tunnels excavated in squeezing ground conditions.

8.2. Application of the proposed criterion

The LDP for the supported tunnel presented is limited to tunnel excavated in the synthetic mudstone specimen and squeezing ground conditions. The scale effect considerations and the similitude theory explain that the tunnel deformations can be normalized with the tunnel radius and will be independent of the size of the tunnel (refer to Appendices A and B). The criterion proposed is only valid in case no damage occurs in the rock mass due to excavation. Fig. 9 shows the post-test picture of the cubical rock specimen. It can be clearly seen that the rock around the excavated tunnel boundary was undamaged even after the five loading stages.

The LDP was found to be in good agreement with the experimental observations in conjunction with excellent coefficients of determination. Future work will calibrate the proposed LDP against different rock properties and the long-term behavior of the squeezing tunnels particularly using field case histories. This will provide the effect of the change in excavation geometry, tunnel support system and rock properties on the LDP model parameters.

8.3. Stress path difference

In the tunnel construction process, the convergence at the boundary is due to an increase in the deviatoric component of stress, i.e. the difference between an increasing tangential stress component and a decreasing radial stress component due to the advancement of the tunnel. If the tunnel is constructed in squeezing ground conditions, the tunnel can converge gradually even after the excavation stage, and without any further stress release due to unloading at the tunnel boundary.

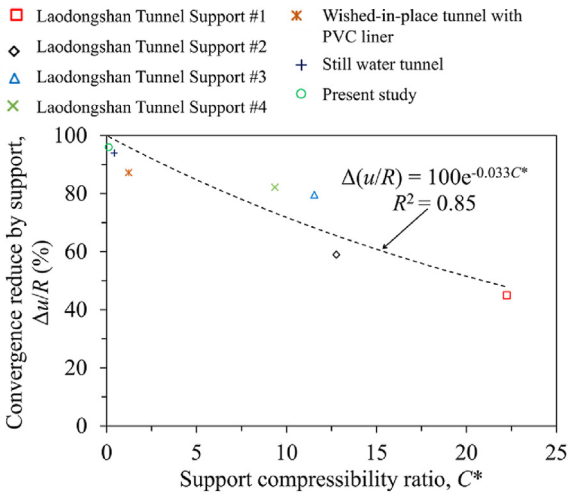

Fig. 8. Plot of $\Delta(u/R)$ versus support compressibility ratio for the case studies presented in Table 3 with the best fit curve.

Fig. 9. Post-test image of a cubical rock specimen with the excavated tunnel and its support system.

The testing procedure described in this research allows for the application of the isotropic stress on cubical rock specimen having cylindrical cavity (tunnel) while monitoring the deformations with time. Although this testing procedure does not replicate the unloading at the tunnel boundary, it effectively simulates the squeezing conditions observed in tunnels. The primary focus of this paper was to monitor the convergence of tunnel with time and develop a criterion that could be applicable to the field, despite the differences in the stress paths.

9. Conclusions

The study presented in this paper developed a novel physical model test to observe supported tunnel closure over time in squeezing ground conditions. The physical model simulated the TBM excavation in a tunnel as it advanced, and time-dependent strains developed due to rock-support interaction after the excavation were monitored. Also, analysis of the data from the strain gauges on the liner provided a quantitative assessment of the LDP of the supported tunnel at different times and stress levels.

Based on the experimental observations, a model was proposed to express the LDP of the tunnel as a function of time. The LDP parameters were found to be a function of the ratio of the isotropic stress applied to the UCS of the rock specimen and the normalized distance from the tunnel face. The LDP parameters of supported and unsupported tunnels were compared to account for the influence of the support system. The back-calculation of thrust forces on the support system provided an estimate of the additional thrust forces in the support due to squeezing. A relationship between convergence, reduced by the support, and support compressibility, was established based on the literature and the present study's observations. A methodology was proposed for the efficient design of the tunnel support system in squeezing ground conditions.

Declaration of competing interest

The authors declare that they have no known competing financial interests or personal relationships that could have appeared to influence the work reported in this paper.

Acknowledgments

The authors gratefully acknowledge the financial support of the University Transportation Center for Underground Transportation Infrastructure (UTC-UTI) at the Colorado School of Mines under Grant No. 69A3551747118 from the US Department of Transportation (DOT). The opinions expressed in this paper are those of the authors and not of the DOT.

Appendix A. Supplementary data

Supplementary data to this article can be found online at https://doi.org/10.1016/j.jrmge.2021.08.016.

References

Alejano, L.R., Rodriguez-Dono, A., Alonso, E., Manín, G.F., 2009. Ground reaction curves for tunnels excavated in different quality rock masses showing several types of post-failure behaviour. Tunn. Undergr. Space Technol. 24 (6), 689–705.
Arora, K., Gutierrez, M., Hedayat, A., 2020a. Experimental setup for studying tunnels in squeezing ground conditions. In: Tunnels and Underground Cities: Engineering and Innovation Meet Archaeology, Architecture and Art, 7. CRC Press. Long and Deep Tunnels.
Arora, K., Gutierrez, M., Hedayat, A., 2020b. Physical modeling of lined tunnel in squeezing ground conditions. In: Geo-Congress 2020: Engineering, Monitoring, and Management of Geotechnical Infrastructure. American Society of Civil Engineers, Reston, VA, USA, pp. 335–344.
Arora, K., Cruz, E.C., Gutierrez, M., Hedayat, A., 2020c. Characterization of synthetic mudstone for physical model studies. In: Proceedings of the 54th US Rock Mechanics/Geomechanics Symposium. American Rock Mechanics Association (ARMA).
Arora, K., Gutierrez, M., Hedayat, A., 2019. Miniature Tunnel boring machine for simulating tunnel excavation in squeezing ground conditions. In: Proceedings of the 4th International Conference on Tunnel Boring Machine in Difficult Ground, pp. 183–192. Denver, Colorado, USA.
Arora, K., 2020. Experimental Study of Tunnels in Squeezing Ground Conditions. PhD Thesis. Colorado School of Mines, Golden, Colorado, USA.
Arora, K., Gutierrez, M., Hedayat, A., 2021a. New physical model to study tunnels in squeezing clay-rich rocks. Geotech. Test J. 44 (6), 1–21.
Arora, K., Gutierrez, M., Hedayat, A., Cruz, E.C., 2021b. Time-dependent behavior of the tunnels in squeezing ground: an experimental study. Rock Mech. Rock Eng. 54 (4), 1755–1777.
Arora, K., Gutierrez, M., Hedayat, A., Xia, C., 2021c. Tunnels in squeezing clay-rich rocks. Undergr. Space 6 (4), 432–445.
Brown, E.T., Bray, J.W., Ladanyi, B., Hoek, E., 1983. Ground response curves for rock tunnels. J. Geotech. Eng. 109 (1), 15–39.
Cai, Y., Jiang, Y., Djamaluddin, I., Iura, T., Esaki, T., 2015. An analytical model considering interaction behavior of grouted rock bolts for convergence–confinement method in tunneling design. Int. J. Rock Mech. Min. Sci. 76, 112–126.
Cao, C., Shi, C., Lei, M., Yang, W., Liu, J., 2018. Squeezing failure of tunnels: a case study. Tunn. Undergr. Space Technol. 77, 188–203.
Carranza-Torres, C., Fairhurst, C., 2000. Application of the convergence–confinement method of tunnel design to rock masses that satisfy the Hoek–Brown failure criterion. Tunn. Undergr. Space Technol. 15 (2), 187–213.
Corbetta, F., Bernaud, D., Minh, D.N., 1991. Contribution à la méthode convergence-confinement par le principe de la similitude. Rev. Fr. Geotech. 54, 5–11 (in French).
Cui, L., Zheng, J.J., Zhang, R.J., Lai, H.J., 2015. A numerical procedure for the fictitious support pressure in the application of the convergence–confinement method for circular tunnel design. Int. J. Rock Mech. Min. Sci. 78, 336–349.
Czurda, K., Winder, C.G., Quigley, R.M., 1973. Sedimentology, mineral facies, and petrofabric of the meaford–dundas formation (upper ordovician) in southern ontario. Can. J. Earth Sci. 10 (12), 1790–1804.
Duncan-Fama, M.E., 1993. Numerical modelling of yield zones in weak rocks. In: Comprehensive Rock Engineering. Pergamon, pp. 49–75.
Fenner, R., 1938. Untersuchungen zur Erkenntis des Gebirgsdruckes bluckauf. Gluckauf 74, 671–695 (in German).
Frash, L., Gutierrez, M., Hampton, J., 2014. True-triaxial apparatus for simulation of hydraulically fractured multi-borehole hot dry rock reservoirs. Int. J. Rock Mech. Min. Sci. 70, 496–506.
Gschwandtner, G.G., Galler, R., 2012. Input to the application of the convergence confinement method with time-dependent material behaviour of the support. Tunn. Undergr. Space Technol. 27 (1), 13–22.
Hoek, E., Marinos, P., 2000. Predicting tunnel squeezing problems in weak heterogeneous rock masses. Tunnels Tunn. Int. 32 (11), 45–51.
Lin, P., Liu, H., Zhou, W., 2015. Experimental study on failure behaviour of deep tunnels under high in-situ stresses. Tunn. Undergr. Space Technol. 46, 28–45.
Liu, B., Yang, H., Karekal, S., 2020. Reliability analysis of TBM disc cutters under different conditions. Undergr. Space 6 (2), 142–152.
Lo, K.Y., Cooke, B.H., Dunbar, D.D., 1987. Design of buried structures in squeezing rock in Toronto, Canada. Can. Geotech. J. 24 (2), 232–241.
Lombardi, G., 1975. Qualche aspetto particolare della statica delle cavita sotterranee. Riv. Ital. Geotec. 2, 187–206 (in Italian).
Lü, Q., Xiao, Z.P., Ji, J., Zheng, J., Shang, Y.Q., 2017. Moving least squares method for reliability assessment of rock tunnel excavation considering ground-support interaction. Comput. Geotech. 84, 88–100.
Nomoto, T., Imamura, S., Hagiwara, T., Kusakabe, O., Fujii, N., 1999. Shield tunnel construction in centrifuge. J. Geotech. Geoenviron. Eng. 125 (4), 289–300.
Pacher, F., 1964. Deformationsmessungen im Versuchsstollen als Mittel zur Erforschung des Gebirgsverhaltens und zur Bemessung des Ausbaues. In: Grundfragen auf dem Gebiete der Geomechanik/Principles in the Field of Geomechanics. Springer, Berlin, Heidelberg, pp. 149–161 (in German).
Pandit, B., Babu, G.S., 2021. Probabilistic stability assessment of tunnel-support system considering spatial variability in weak rock mass. Comput. Geotech. 137, 104242.
Panet, M., 1995. Calcul des tunnels par la me'thode de convergence–confinement, 178. Presses de l'Ecole Nationale des Ponts et Chausse'es, Paris, pp. 11–19 (in French).
Panet, M., 1993. Understanding deformations in tunnels. Comp. Rock Eng. 1, 663–690.
Paraskevopoulou, C., Benardos, A., 2013. Assessing the construction cost of Greek transportation tunnel projects. Tunn. Undergr. Space Technol. 38, 497–505.
Paraskevopoulou, C., Diederichs, M., 2018. Analysis of time-dependent deformation in tunnels using the convergence-confinement method. Tunn. Undergr. Space Technol. 71, 62–80.
Peila, D., Oreste, P.P., 1995. Axisymmetric analysis of ground reinforcing in tunnelling design. Comput. Geotech. 17 (2), 253–274.
Schwartz, C.W., Einstein, H.H., 1980. Improved design of tunnel supports. Technical Report. In: Simplified Analysis for Ground-Structure Interaction in Tunneling, 1. Urban Mass Transportation Administration, USA. report.
Vrakas, A., Anagnostou, G., 2014. A finite strain closed-form solution for the elastoplastic ground response curve in tunnelling. Int. J. Num. Anal. Meth. Geomech. 38 (11), 1131–1148.
Wang, S.F., Zhang, Z.X., Huang, X., 2019. Physical modelling on the cutterhead-block interaction during TBM tunneling. In: Proceedings of the 53rd US Rock Mechanics/Geomechanics Symposium. American Rock Mechanics Association (ARMA), pp. 45–50.
Zhang, P., Nordlund, E., 2021. A 3DEC numerical analysis of the interaction between an uneven rock surface and shotcrete lining. Rock Mech. Rock Eng. 54 (5), 2267–2289.

Dr. Ketan Arora is currently working as a Tunnel Engineer for Aldea Services Inc. and adjunct faculty at Colorado School of Mines. Prior to this, Dr. Arora has worked as a Post-Doctoral Researcher in the Department of Civil and Environmental Engineering at the Colorado School of Mines. He received his PhD in 2020 from Colorado School of Mines, MTech with specialization in Rock Engineering and Underground Structures from IIT Delhi in 2016, and BTech in Civil Engineering from NIT Surat in 2014. Dr. Arora's teaching and research interests focus on Experimental Geomechanics, Geomaterials Characterization, Rock Mechanics, Instrumentation and Monitoring, and Underground Construction. Dr. Arora's research aims at addressing some of the fundamental issues of geotechnical engineering as applied to tunnels and underground structures through laboratory tests. In the last six years, Dr. Arora has advanced the knowledge of rocks' engineering behavior and their applications in underground structures such as tunnels. Dr. Arora has experience conducting conventional laboratory tests on the rock specimen and designing a novel test method.